Macromolecules

ARTICLE

pubs.acs.org/Macromolecules

Polymer Crystallization of Partially Miscible Polythiophene/Fullerene Mixtures Controls Morphology

Derek R. Kozub,[†] Kiarash Vakhshouri,[†] Lisa M. Orme,[†] Cheng Wang,[‡] Alexander Hexemer,[‡] and Enrique D. Gomez*[,†,§]

[†]Department of Chemical Engineering, The Pennsylvania State University, University Park, Pennsylvania 16802, United States

[‡]Advanced Light Source, Lawrence Berkeley National Laboratory, Berkeley, California 94530, United States

[§]Materials Research Institute, The Pennsylvania State University, University Park, Pennsylvania 16802, United States

Supporting Information

ABSTRACT: Mixtures of polythiophene and fullerene are intensely studied for organic photovoltaic applications. Control of nanoscale morphology of these materials is critical for device performance, but characterization and understanding of this morphology and how it arises is lacking. We use energy-filtered transmission electron microscopy (EFTEM) to obtain high-contrast images of P3HT nanocrystals in organic semiconductor mixtures. Grazing-incidence small-angle X-ray scattering correlates well with the length scales obtained from EFTEM images; we combine the two techniques to follow the morphology evolution under different material processing histories. EFTEM also measures local P3HT concentration in PCBM-rich regions, proving that these components are partially miscible. We determine the P3HT-PCBM χ parameter and Flory−Huggins phase diagram, which predicts miscibility for P3HT volume fractions above 0.42. This miscibility suppresses fullerene crystallization. The nanoscale morphology in these materials, critical for solar cell performance, is driven by P3HT crystallization from a partially miscible blend.

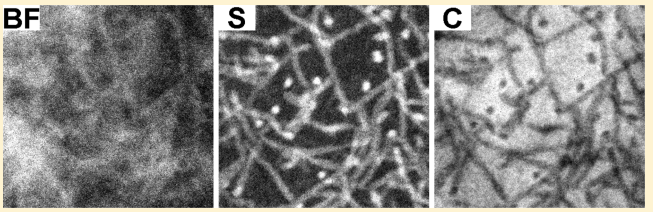

INTRODUCTION

Electron donor/acceptor mixtures of organic conjugated molecules have the potential to serve as the active layer in large-area, low-cost, and flexible solar cells.[1−4] The morphology of the organic semiconductor mixture, critical for efficient device performance, is a result of the interplay between the crystallinity and the chemical incompatibility of the constituents. Our current understanding of organic semiconductors suggests intricate nanoscale morphologies are necessary to achieve high-performance devices.[5−10] Large amounts of electron donor/acceptor interfaces promote charge separation, bicontinuous domains lead to efficient charge transport, and domain sizes on the order of the exciton diffusion length (5−10 nm[11]) prevent exciton decay. Previous efforts have established a strong dependence of the device performance of bulk heterojunction organic solar cells on the processing conditions of the active layer.[1,2,4−6,12−15] Regardless, a direct connection between the active layer morphology and device performance is lacking. Achieving device efficiencies in excess of 10%, important for widespread commercialization of organic solar cells,[2,16] will require a basic understanding of the factors governing structural evolution in organic semiconductor mixtures to select the optimum molecular properties and processing conditions.

Characterization of the phase separation in organic semiconductor mixtures has been a strong focus of recent work.[5,6,8,12,13,17−22] In devices made from poly(3-hexylthiophene-2,5-diyl) (P3HT) and [6,6]-phenyl-C_{61} butyric acid methyl ester (PCBM), direct imaging of the composite films has been attempted through atomic force microscopy (AFM)[6,12,15] and transmission electron microscopy (TEM).[6,12,13,17] However, contrast is weak in TEM images, and the origin of contrast is not clear in either of these techniques. Furthermore, AFM is a surface-sensitive technique, and recent work has shown that P3HT selectively wets the air surface of P3HT:PCBM films.[23,24] Morphological characterization of semiconductor mixtures utilized in organic photovoltaics remains a challenge, and consequently, the factors governing structural evolution remain poorly understood.

Here, we report the use of energy-filtered transmission electron microscopy (EFTEM) to generate high contrast images of the morphology in polythiophene/fullerene mixtures. Furthermore, elemental maps depict the local elemental composition of the domains. In conjunction with complementary data from grazing-incidence small-angle X-ray scattering (GISAXS), EFTEM images allow us to examine the morphology evolution. Our approach, widely applicable to many organic semiconductor mixtures, enables characterization of the phase separation and morphology in thin films with varying degrees of long-range order.

Received: April 13, 2011
Revised: June 16, 2011
Published: June 30, 2011

We demonstrate that a significant amount of uncrystallized polymer exists as a homogeneous polythiophene/fullerene mixture among rod-like polythiophene crystals. Elemental analysis of the amorphous regions demonstrates partial miscibility of P3HT and PCBM. By determining the interaction parameter, χ, and the Flory−Huggins phase diagram, we predict miscibility for P3HT volume fractions greater than 0.42. We find miscibility to suppress fullerene crystallization. The combination of miscibility and suppression of fullerene crystallization at compositions near the optimum for solar cells (~0.6 volume fraction P3HT)[20,21,25] suggests that the nanoscale morphology, and consequently the device performance, is driven by polymer crystallization from partially miscible blends.

EXPERIMENTAL METHODS

Solutions of regioregular P3HT (96% H−T regioregular, M_n = 28 kg/mol, polydispersity =1.9, Merck), regiorandom P3HT (M_n = 30 kg/mol, polydispersity =3, Sigma-Aldrich) and PCBM (>99.5%, Nano-C) were made with anhydrous chlorobenzene (Sigma-Aldrich) in a N_2 glovebox. Solutions were stirred for a minimum of 1 h and heated to 100 °C for 10 s prior to use to ensure dissolution.

To simulate conditions relevant to polymer solar cells, thin films of P3HT:PCBM were cast on 100 nm poly(3,4-ethylenedioxythiophene) poly(styrenesulfonate), PEDOT:PSS, (Clevios P, H. C. Starck) films deposited on silicon wafers. Silicon wafers were cleaned through sonication for 10 min in acetone and isopropanol followed by 10 min of UV−ozone treatment. Thin films (ca. 70 ± 10 nm) for TEM experiments were made by spin coating 15 mg/mL P3HT:PCBM solutions in a N_2 glovebox at 1000 rpm for 1 min. Films were subsequently floated-off in distilled water and picked up with copper TEM grids. Samples were dried for 24 h under vacuum and subsequently annealed on a calibrated digital hot plate in a N_2 glovebox. Films were rapidly cooled to room temperature after annealing was complete by placing them on a metal surface.

TEM experiments took place at the National Center for Electron Microscopy, Lawrence Berkeley National Laboratory, on a Zeiss LIBRA 200MC. Bright field images, thickness maps and elemental maps were captured. Sulfur and carbon elemental maps were obtained through the standard three-window method.[26]

Grazing incidence small angle X-ray scattering (GISAXS) experiments were conducted on beamline 7.3.3 at the Advanced Light Source, Lawrence Berkeley National Laboratory (λ = 1.24 Å). In a similar manner as for TEM samples, P3HT:PCBM thin films (ca. 152 ± 11 nm) were spun-cast on PEDOT:PSS/silicon substrates from 24 mg/mL solutions. Samples were annealed on the PEDOT:PSS/silicon substrate inside the N_2 glovebox. GISAXS data was taken at angles above the critical angle for 1:1 P3HT:PCBM mixtures (0.135°) but below the silicon critical angle (0.21°).[27] In-plane data was corrected for scattering from air and the substrate as described in the GISAXS data reduction section of the Supporting Information.

Samples for differential scanning calorimetry experiments (Q1000, TA Instruments) were made by mixing P3HT and PCBM together at various concentrations. Scans were performed from 40 to 300 °C at 5 °C/min.

RESULTS AND DISCUSSION

Although P3HT:PCBM mixtures have been intensively studied,[4,7,13,17,22−25,28−35] the extent of miscibility and the domain compositions remain unknown. By taking advantage of inelastic losses due to electron-sample interactions in the electron microscope, EFTEM allows for mapping of the local elemental composition through the standard three-window method.[36] The active layers of polythiophene/fullerene solar cells are ideal candidates for elemental mapping due to the large differences in sulfur and carbon densities between P3HT and PCBM. Indeed, the sulfur and carbon elemental maps show more contrast than the bright field image in Figure 1. The intensity of the elemental maps is directly proportional to the elemental concentration within domains.[36] The rod-like P3HT crystallites are clearly visible in the elemental maps as light and dark regions in the sulfur and carbon maps, respectively.

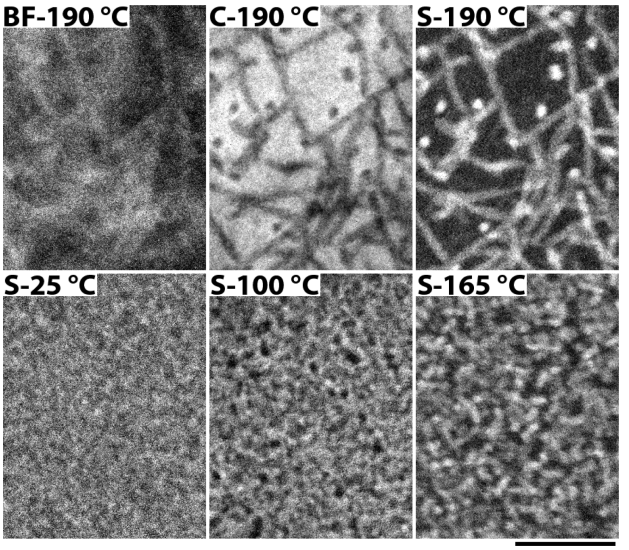

Figure 1. Top: Bright field (BF), sulfur map (S), and carbon map (C) for a 1:1 P3HT/PCBM film annealed for 30 min. The same region of the sample is shown and images were taken at zero defocus. Bottom: Sulfur maps of 1:1 P3HT/PCBM films annealed at 25 °C, 100 °C, and 165 °C. The image intensities of sulfur maps are proportional to the sulfur concentration and the light regions correspond to P3HT-rich domains. Unannealed films (25 °C) show little structure, while films annealed at high temperatures, such as 190 °C, exhibit the presence of P3HT fibers in a PCBM-rich matrix. Scale bar: 200 nm.

Analysis of the contrast in both sulfur and carbon elemental maps shown in Figure 1 allows us to determine that the fibers are essentially pure P3HT (99 ± 8%) and the PCBM-rich regions contain 45 ± 4% P3HT by volume in a 1:1 by mass mixture annealed at 190 °C for 30 min. The concentration of the PCBM-rich region is consistent with the volume fraction of fibers visible at 190 °C in Figure 1 (see Supporting Information for further details). Little or no structure is visible in the PCBM-rich regions, demonstrating that P3HT and PCBM can be molecularly mixed. Furthermore, annealing films at 200 °C leads to films with no mesoscopic structure (Figure S1). Thus, the EFTEM results suggest that P3HT and PCBM are miscible.

Elemental mapping is a powerful technique for examining the structural evolution in polythiophene/fullerene mixtures, as shown in the bottom panel of Figure 1. As cast films show little structure, while P3HT fibers are clearly visible for films annealed at 165 and 190 °C. Although increasing the annealing temperature increases the fiber length and fiber diameter (Figure S4), the concentration of fibers also decreases (see Supporting Information for details). The presence of fiber-like P3HT crystals throughout P3HT:PCBM mixtures suggests that the P3HT crystallization dominates the mesostructure formation process.

We can complement and confirm our measurements of morphological evolution in polythiophene/fullerene mixtures through GISAXS. Grazing-incidence X-ray scattering is widely

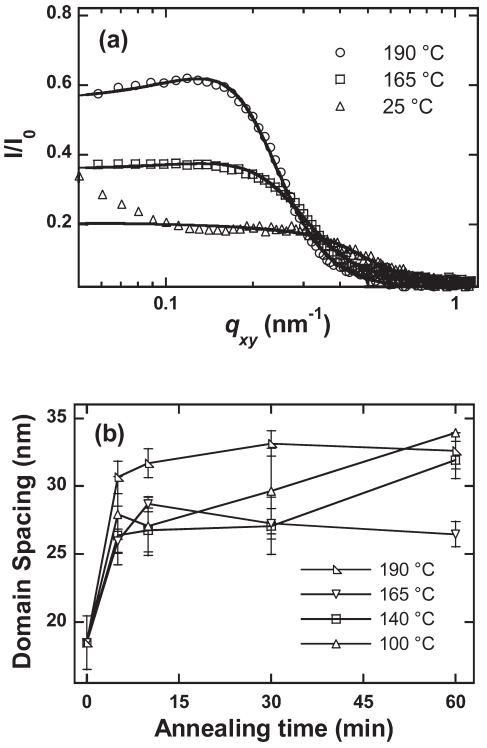

Figure 2. (a) GISAXS intensity vs in-plane scattering vector, q_{xy} for 1:1 P3HT:PCBM mixtures annealed at various temperatures for 30 min. The solid lines are Teubner−Strey fits to the data. (b) Domain spacings from GISAXS data of 1:1 P3HT:PCBM mixtures at various annealing conditions. Note that films annealed at 165 and 190 °C appear to approach a steady state within the time scale of our experiments. Lines are guides to the eye. Error bars denote the standard deviation of multiple measurements.

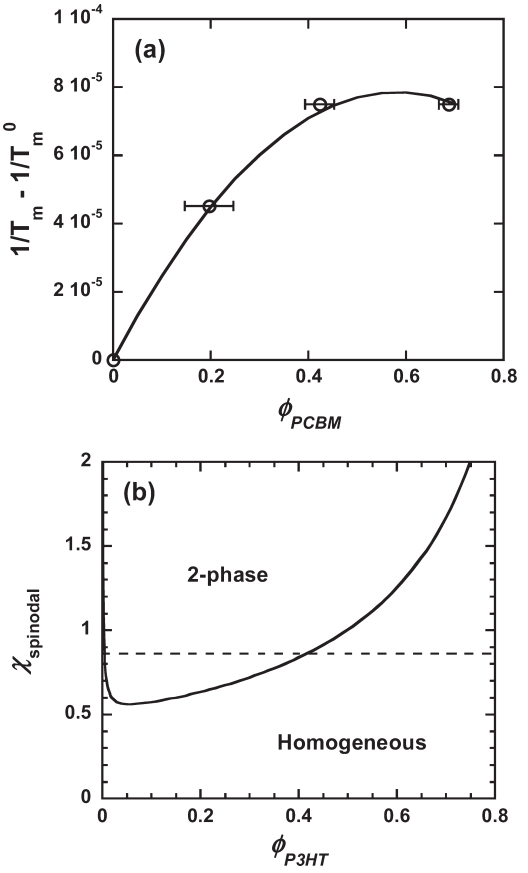

Figure 3. Estimate of the miscibility from measurements of the melting point depression. (a) Melting point depression of P3HT as a function of PCBM volume fraction, φ_{PCBM}, obtained from DSC experiments. The solid line is from eq 1 with $\chi = 0.86$. Error bars represent the uncertainty in composition due to the limited accuracy of the scale. (b) Spinodal as a function of P3HT volume fraction, φ_{P3HT}, obtained by modeling P3HT:PCBM mixtures as polymer solutions with $MW^{P3HT} = 50\,000$ g/mol. The dotted line denotes $\chi = 0.86$, and in combination with the spinodal indicates that homogeneous P3HT:PCBM mixtures are unstable for $\varphi_{P3HT} < 0.42$.

utilized to study the structure of polymer thin films.[5,7,33,37−39] In GISAXS, the scattering is acquired in the reflection geometry with incident angles near the critical angle of the film to minimize the contribution of the substrate to the scattering intensities.[37,40] With this technique, a quantitative measure of the mesostructure in organic semiconductor mixtures can be obtained.

Figure 2a shows the GISAXS intensity as a function of the in-plane scattering vector, q_{xy}, for films annealed at various temperatures for 30 min. Consistent with the sulfur elemental map shown in Figure 1, little structure is apparent after the film is cast prior to thermal annealing. This suggests that the film-casting process briefly plasticizes the film and allows for limited crystallization of P3HT to occur.[7] Annealing leads to the formation of structure, as evident in the increase in the scattering intensity at low q after thermal annealing. The intensities, however, approach a finite value as q approaches zero, suggesting little macroscale phase separation is present after annealing.

Extracting structural parameters of the morphology from GISAXS intensities requires fitting to a model. The morphologies visible in Figure 1 are poorly ordered yet possess a characteristic length scale corresponding to the P3HT crystal dimension; visually, they resemble polymer microemulsions.[41] As shown by the solid curves in Figure 2a, the use of the Teubner−Strey scattering function, originally developed for oil/water/microemulsions[42] and later extended to polymer blends,[43,44] describes the GISAXS data well over a wide q-range for samples annealed at elevated temperatures. The upturn in the intensities at low-q of the scattering data from as-cast films prior to thermal annealing is not captured by Teubner−Strey and is most likely due to macrophase separation or structures larger than 150 nm. Thus, we assume that Teubner−Strey is an appropriate model for describing the mesostructure visible in Figure 1 for unannealed P3HT:PCBM films (details of the fitting procedure can be found in the Supporting Information). Figure 2a demonstrates that Teubner−Strey is an appropriate model for describing scattering from P3HT:PCBM films.

Using Teubner−Strey as a model for the scattering data, the morphology in terms of the domain spacing, d, can be quantified. We examined films annealed at 100, 140, 165, and 190 °C for 5, 10, 30, and 60 min, as shown in Figure 2b. At 100 and 140 °C, the domain spacing grows with time, suggesting coarsening of the structure. At 165 and 190 °C, however, d increases quickly and then appears to approach a steady state. It is surprising that further coarsening is strongly suppressed or does not occur at elevated temperatures.

We can obtain a direct measure of the chemical interactions by measuring the melting point depression of P3HT in P3HT:PCBM mixtures. Through differential scanning calorimetry, we

dx.doi.org/10.1021/ma200855r |*Macromolecules* 2011, 44, 5722–5726

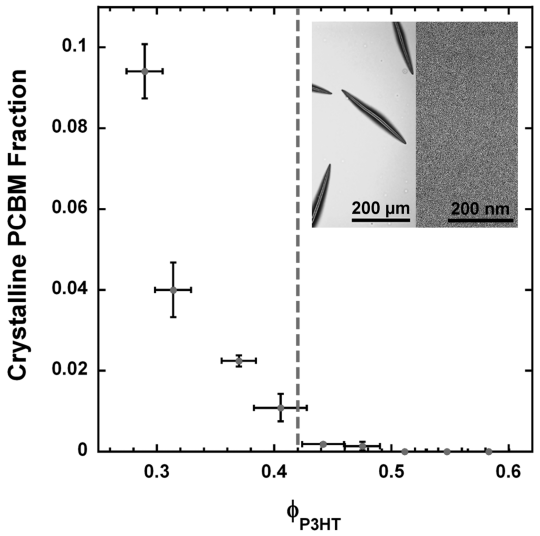

Figure 4. PCBM crystallization in regiorandom P3HT:PCBM films as a function of φ_{P3HT}. The dotted line corresponds to $\varphi_{P3HT} = 0.42$. PCBM crystallization is estimated from the area fraction of PCBM crystals visible in optical micrographs (inset, left). The film shown in the optical micrograph ($\varphi_{P3HT} = 0.37$) was annealed at 190 °C for 30 min. Sulfur elemental maps indicate that the films are homogeneous at nanometer length scales (inset, right). The sulfur map shown is of a regiorandom P3HT:PCBM film with $\varphi_{P3HT} = 0.58$ annealed at 190 °C for 30 min. Note that Figure 3 predicts P3HT:PCBM mixtures to be miscible for $\varphi_{P3HT} > 0.42$. Error bars denote the standard deviation of multiple measurements.

can obtain an estimate of the Flory−Huggins interaction parameter, χ, using eq 1:[45]

$$\frac{1}{T_m} - \frac{1}{T_m{}^0} = \frac{R}{\Delta H_f}\frac{v_m}{v_s}(\phi_s - \chi\phi_s{}^2) \qquad (1)$$

where T_m is the melting point at a solvent (PCBM) volume fraction φ_s, $T_m{}^0$ is the melting point of pure polymer, R is the ideal gas constant, ΔH_f is the heat of fusion of polymer, v_m is the monomer molar volume of polymer ($v_{m,P3HT} = 151$ cm^3/mol)[46] and v_s is the solvent molar volume ($v_{s,PCBM} = 607$ cm^3/mol).[47] ΔH_f is obtained from the melting endotherm. Fitting eq 1 to the melting point data shown in Figure 3a with χ as the only adjustable parameter yields $\chi = 0.86 \pm 0.09$. The error in χ is estimated from the uncertainty of the fit. From the Flory−Huggins free energy of mixing equation for polymer solutions,[48] we obtain the spinodal, shown in Figure 3b. The combination of the spinodal and χ allows for the determination of the miscibility of amorphous P3HT:PCBM mixtures. We find that for P3HT concentrations greater than 0.42 by volume, the mixtures are miscible. Therefore, the structure present in 1:1 by mass mixtures ($\varphi_{P3HT} = 0.58$) utilized in both the experiments illustrated in Figures 1−3 and in organic solar cells commonly reported in the literature[2,16] is not a result of demixing of the amorphous phases, but instead, must be a consequence of polymer crystallization.

Thus, the results in Figures 1−3 lead to the conclusion that polymer crystallization drives the structure formation process in miscible polythiophene/fullerene mixtures. As-cast films have little structure, as evident in Figures 1 and 2. Annealing enhances molecular motion and allows polythiophene to precipitate as a crystalline pure phase, rejecting PCBM to the amorphous mixed phase. Therefore, polymer crystallization enhances the concentration of PCBM in the amorphous phase and leads to macroscopic phase separation if enough polymer crystallization takes place. This conclusion is consistent with the micrometer-sized fullerene clusters visible through optical microscopy of 1:1 by mass P3HT:PCBM mixtures after thermal annealing,[8] the mesostructure visible in Figure 1 through EFTEM, and recent evidence from dynamic secondary ion mass spectrometry that suggests P3HT and PCBM are not completely immiscible.[28] Thus, our results provide an explanation for the amorphous nature of micrometer-sized fullerene clusters often observed in 1:1 by mass polythiophene/fullerene mixtures[5,7,38,49]—the formation of the fullerene clusters is not driven by the crystallization of fullerene but rather by a combination of P3HT crystallization and the limited solubility of P3HT and PCBM. Assuming an upper limit for P3HT crystallization of 40%,[50] we surmise that the upper limit of fullerene loading prior to cluster formation is 45% PCBM by volume for annealed semicrystalline films. Furthermore, the observed correlation between the P3HT and PCBM crystallinity[5] is most likely from the enhancement of the PCBM local concentration due to the crystallization of P3HT.

Our results suggest that the crystallization of PCBM would be suppressed in mixtures of amorphous P3HT with PCBM if $\varphi_{P3HT} > 0.42$. To test this hypothesis, we mixed regiorandom P3HT, which does not crystallize, with PCBM and examined the film morphology. Figure 4 shows the PCBM crystallization as the area fraction of PCBM crystals visible in optical micrographs for films with varying composition. For regiorandom P3HT concentrations above 0.42, when the mixture is miscible, no evidence of microstructure is observed through elemental mapping even after annealing for 30 min at 190 °C (inset of Figure 4). Consistent with the Flory−Huggins phase diagram shown in Figure 3, the crystallization of fullerene is strongly suppressed at φ_{P3HT} above 0.42.

CONCLUSIONS

In summary, we have shown that the intricate mesoscopic structure of polythiophene/fullerene mixtures, critical for device performance, is driven by the crystallization of the polymer. Quantifying the chemical interactions between P3HT and PCBM through the Flory−Huggins interaction parameter enables the determination of the extent of miscibility between these two components when they are amorphous. Miscibility between P3HT and PCBM suppresses fullerene crystallization. The crystallization of the polymer leads to the characteristic length scales of the mesostructure, whereby crystallization of the polymer can also lead to macroscopic phase separation by enriching the amorphous polymer phase with fullerene beyond the miscibility limit. Therefore, the volume fraction of the pure PCBM phase should correlate to the crystallinity of P3HT in the mixture. By providing a description of the structure formation process in polythiophene/fullerene blends, our results may lead to strategies for controlling the morphology in organic semiconductor mixtures utilized in the active layer of solar cells.

ASSOCIATED CONTENT

Supporting Information. Detailed information on the analysis of elemental maps, GISAXS data reduction, and comparison between the GISAXS and EFTEM data. This material is free of charge via the Internet at http://pubs.acs.org.

■ ACKNOWLEDGMENT

The authors gratefully acknowledge Scott Milner for helpful discussion and suggestions. MRSEC funding through the NSF-sponsored Center for Nanoscale Science at the Pennsylvania State University is acknowledged. Funding from the Oakridge Associated Universities Ralph E. Powe Junior Faculty Enhancement Award is also acknowledged. The authors acknowledge support of the National Center for Electron Microscopy, Lawrence Berkeley National Laboratory, which is supported by the U.S. Department of Energy under Contract no. DE-AC02-05CH11231. The Advanced Light Source is supported by the Director, Office of Science, Office of Basic Energy Sciences, of the U.S. Department of Energy under Contract No. DE-AC02-05CH11231.

■ REFERENCES

(1) Li, G.; Shrotriya, V.; Yao, Y.; Huang, J. S.; Yang, Y. *J. Mater. Chem.* **2007**, *17* (30), 3126–3140.
(2) Brabec, C. J.; Gowrisanker, S.; Halls, J. J. M.; Laird, D.; Jia, S.; Williams, S. P. *Adv. Mater.* **2010**, *22* (34), 3839–3856.
(3) Shaheen, S. E.; Ginley, D. S.; Jabbour, G. E. *MRS Bull.* **2005**, *30* (1), 10–19.
(4) Thompson, B. C.; Fréchet, J. M. J. *Angew. Chem., Int. Ed.* **2008**, *47* (1), 58–77.
(5) Woo, C. H.; Thompson, B. C.; Kim, B. J.; Toney, M. F.; Frechet, J. M. J. *J. Am. Chem. Soc.* **2008**, *130* (48), 16324–16329.
(6) Xin, H.; Reid, O. G.; Ren, G. Q.; Kim, F. S.; Ginger, D. S.; Jenekhe, S. A. *ACS Nano* **2010**, *4* (4), 1861–1872.
(7) Gomez, E. D.; Barteau, K. P.; Wang, H.; Toney, M. F.; Loo, Y.-L. *Chem. Commun.* **2011**, *47* (1), 436–438.
(8) Campoy-Quiles, M.; Ferenczi, T.; Agostinelli, T.; Etchegoin, P. G.; Kim, Y.; Anthopoulos, T. D.; Stavrinou, P. N.; Bradley, D. D. C.; Nelson, J. *Nat. Mater.* **2008**, *7* (2), 158–164.
(9) Burkhard, G. F.; Hoke, E. T.; Scully, S. R.; McGehee, M. D. *Nano Lett.* **2009**, *9* (12), 4037–4041.
(10) Coffey, D. C.; Reid, O. G.; Rodovsky, D. B.; Bartholomew, G. P.; Ginger, D. S. *Nano Lett.* **2007**, *7* (3), 738–744.
(11) Haugeneder, A.; Neges, M.; Kallinger, C.; Spirkl, W.; Lemmer, U.; Feldmann, J.; Scherf, U.; Harth, E.; Gugel, A.; Mullen, K. *Phys. Rev. B* **1999**, *59* (23), 15346–15351.
(12) Ma, W.; Yang, C.; Gong, X.; Lee, K.; Heeger, A. J. *Adv. Funct. Mater.* **2005**, *15* (10), 1617–1622.
(13) van Bavel, S. S.; Sourty, E.; de With, G.; Loos, J. *Nano Lett.* **2009**, *9* (2), 507–513.
(14) Yang, F.; Shtein, M.; Forrest, S. R. *Nat. Mater.* **2005**, *4* (1), 37–41.
(15) Li, G.; Shrotriya, V.; Huang, J. S.; Yao, Y.; Moriarty, T.; Emery, K.; Yang, Y. *Nat. Mater.* **2005**, *4* (11), 864–868.
(16) Dennler, G.; Scharber, M. C.; Brabec, C. J. *Adv. Mater.* **2009**, *21* (13), 1323–1338.
(17) Moon, J. S.; Lee, J. K.; Cho, S. N.; Byun, J. Y.; Heeger, A. J. *Nano Lett.* **2009**, *9* (1), 230–234.
(18) Chiu, M. Y.; Jeng, U. S.; Su, C. H.; Liang, K. S.; Wei, K. H. *Adv. Mater.* **2008**, *20* (13), 2573.
(19) Kiel, J. W.; Eberle, A. P. R.; Mackay, M. E. *Phys. Rev. Lett.* **2010**, *105* (16), 168701.
(20) Muller, C.; Ferenczi, T. A. M.; Campoy-Quiles, M.; Frost, J. M.; Bradley, D. D. C.; Smith, P.; Stingelin-Stutzmann, N.; Nelson, J. *Adv. Mater.* **2008**, *20* (18), 3510−3515.
(21) Kim, J. Y.; Frisbie, D. *J. Phys. Chem. C* **2008**, *112* (45), 17726–17736.
(22) Zhao, J.; Swinnen, A.; Van Assche, G.; Manca, J.; Vanderzande, D.; Van Mele, B. *J. Phys. Chem. B* **2009**, *113* (6), 1587–1591.
(23) Xu, Z.; Chen, L. M.; Yang, G. W.; Huang, C. H.; Hou, J. H.; Wu, Y.; Li, G.; Hsu, C. S.; Yang, Y. *Adv. Funct. Mater.* **2009**, *19* (8), 1227–1234.
(24) Germack, D. S.; Chan, C. K.; Hamadani, B. H.; Richter, L. J.; Fischer, D. A.; Gundlach, D. J.; DeLongchamp, D. M. *Appl. Phys. Lett.* **2009**, *94* (23), 233303.
(25) van Bavel, S. S.; Bärenklau, M.; de With, G.; Hoppe, H.; Loos, J. *Adv. Funct. Mater.* **2010**, *20* (9), 1458–1463.
(26) Egerton, R. F., *Electron Energy-Loss Spectroscopy in the Electron Microscope*, 2nd ed.; Plenum Press: New York, NY, 1986.
(27) Diebold, A. C., *Handbook of Silicon Semiconductor Metrology*. Marcel Dekker Inc.: New York, NY, 2001.
(28) Treat, N. D.; Brady, M. A.; Smith, G.; Toney, M. F.; Kramer, E. J.; Hawker, C. J.; Chabinyc, M. L. *Adv. Energy Mater.* **2011**, *1* (1), 82–89.
(29) Wang, X.; Zhang, D.; Braun, K.; Egelhaaf, H. J.; Brabec, C. J.; Meixner, A. J. *Adv. Funct. Mater.* **2010**, *20* (3), 492–499.
(30) Guan, Z. L.; Kim, J. B.; Wang, H.; Jaye, C.; Fischer, D. A.; Loo, Y. L.; Kahn, A. *Org. Electron.* **2010**, *11* (11), 1779–1785.
(31) Gao, Y. Q.; Martin, T. P.; Thomas, A. K.; Grey, J. K. *J. Phys. Chem. Lett.* **2010**, *1* (1), 178–182.
(32) Chiu, M. Y.; Jeng, U. S.; Su, M. S.; Wei, K. H. *Macromolecules* **2010**, *43* (1), 428–432.
(33) Jimison, L. H.; Toney, M. F.; McCulloch, I.; Heeney, M.; Salleo, A. *Adv. Mater.* **2009**, *21* (16), 1568–1572.
(34) Chen, H.-Y.; Yang, H.; Yang, G.; Sista, S.; Zadoyan, R.; Li, G.; Yang, Y. *J. Phys. Chem. C* **2009**, *113* (18), 7946–7953.
(35) Brinkmann, M.; Rannou, P. *Macromolecules* **2009**, *42* (4), 1125–1130.
(36) Egerton, R. F., *Electron energy-loss spectroscopy in the electron microscope*, 2nd ed.; Plenum Press: New York, 1996.
(37) Baker, J. L.; Jimison, L. H.; Mannsfeld, S.; Volkman, S.; Yin, S.; Subramanian, V.; Salleo, A.; Alivisatos, A. P.; Toney, M. F. *Langmuir* **2010**, *26* (11), 9146–9151.
(38) Li, G.; Yao, Y.; Yang, H.; Shrotriya, V.; Yang, G.; Yang, Y. *Adv. Funct. Mater.* **2007**, *17* (10), 1636–1644.
(39) Khanna, V.; Cochran, E. W.; Hexemer, A.; Stein, G. E.; Fredrickson, G. H.; Kramer, E. J.; Li, X.; Wang, J.; Hahn, S. F. *Macromolecules* **2006**, *39* (26), 9346–9356.
(40) Renaud, G.; Lazzari, R.; Leroy, F. *Surf. Sci. Rep.* **2009**, *64* (8), 255–380.
(41) Zhou, N.; Bates, F. S.; Lodge, T. P. *Nano Lett.* **2006**, *6* (10), 2354–2357.
(42) Teubner, M.; Strey, R. *J. Chem. Phys.* **1987**, *87* (5), 3195–3200.
(43) Morkved, T. L.; Stepanek, P.; Krishnan, K.; Bates, F. S.; Lodge, T. P. *J. Chem. Phys.* **2001**, *114* (16), 7247.
(44) Ruegg, M. L.; Reynolds, B. J.; Lin, M. Y.; Lohse, D. J.; Balsara, N. P. *Macromolecules* **2006**, *39* (3), 1125–1134.
(45) Flory, P. J., *Principles of Polymer Chemistry*, 11 ed.; Cornell University Press: Ithaca, NY, 1953.
(46) Prosa, T. J.; Winokur, M. J.; Moulton, J.; Smith, P.; Heeger, A. J. *Macromolecules* **1992**, *25* (17), 4364–4372.
(47) Bulle-Lieuwma, C. W. T.; van Gennip, W. J. H.; van Duren, J. K. J.; Jonkheijm, P.; Janssen, R. A. J.; Niemantsverdriet, J. W. *Appl. Surf. Sci.* **2003**, *203*, 547–550.
(48) Rubinstein, M. C., Ralph, H., *Polymer Physics*; Oxford University Press: New York, 2003.
(49) Chu, C. W.; Yang, H. C.; Hou, W. J.; Huang, J. S.; Li, G.; Yang, Y. *Appl. Phys. Lett.* **2008**, *92* (10), 103306.
(50) Brinkmann, M.; Wittmann, J. C. *Adv. Mater.* **2006**, *18* (7), 860–863.